Phase-Precession-Like Effects in the Anterior Insula Cortex during Reward Expectancy

Linglin Yang[1,2], Katia Lehongre[3], Hongyi Ye[2], Vincent Navarro[4,5,6], Zheng Lin[1], Sen Cheng[7], Nikolai Axmacher[8,9], Shuang Wang[2], Hui Zhang[8]

[1] Department of Psychiatry, Second Affiliated Hospital, School of medicine, Zhejiang University, 310020 Hangzhou, China

[2] Department of Neurology, Epilepsy center, Second Affiliated Hospital, School of medicine, Zhejiang University, 310020 Hangzhou, China

[3] CENIR - Centre de Neuro-Imagerie de Recherche, Paris Brain Institute, ICM, Hôpital de la Pitié-Salpêtrière, 75013 Paris, France

[4] Sorbonne Université, Inserm, CNRS, Paris Brain Institute, ICM, Hôpital de la Pitié-Salpêtrière, 75013 Paris, France

[5] Epilepsy Unit, AP-HP, PitiéSalpêtrière Hospital, 75013 Paris, France

[6] Clinical Neurophysiology Department, AP-HP, Pitié-Salpêtrière Hospital, 75013 Paris, France

[7] Institute for Neural Computation, Faculty of Computer Science, Ruhr University Bochum, 44801 Bochum, Germany

[8] Department of Neuropsychology, Institute of Cognitive Neuroscience, Faculty of Psychology, Ruhr University Bochum, 44801 Bochum, Germany

[9] State Key Laboratory of Cognitive Neuroscience and Learning and IDG/McGovern Institute for Brain Research, Beijing Normal University, 100875 Beijing, PR China

Correspondence
Hui.Zhang-c5u@ruhr-uni-bochum.de (Hui Zhang)
wangs77@zju.edu.cn (Shuang Wang)

Abstract

Reward expectancy contributes to cognitive performance and is governed by the anterior insular cortex (AIC). To investigate the electrophysiological mechanisms underlying reward expectancy in the AIC, we collected intracranial electroencephalography (iEEG) data from epilepsy patients implanted for clinical purposes while they were navigating a virtual T-maze. During navigation, subjects encountered rewards at three pre-defined locations. We focused on the time window proximity to entering the reward zone, which was defined as the reward-expectancy stage. A strong phase-amplitude coupling (PAC) between local theta phase and gamma power within the AIC has been reported at the expectancy stage of rewards. Interestingly, the PAC effect exhibited a specific temporal structure in which the gamma power was progressively coupled to earlier theta phase before each onset of the same reward. Meanwhile, the reward-specific brain patterns were pre-activated during the expectancy stage of rewards, taking place slightly prior to the occurrence of peak gamma activities across individual trials. Furthermore, the pre-activation of reward-specific patterns also progressively shifted forward on theta phases as more trials were conducted. These phenomena of phase shift were reminiscent of the phase precession effect in which single neurons fire at progressively earlier phases of low-frequency oscillations, and thus were called phase-precession-like effects (PPLEs). Additionally, subjects exhibiting PPLEs in the AIC presented less variability and a more notable improvement in response latency across trials. These results indicate that PPLEs in the AIC play an important role in reward expectancy which in turn facilitate task performance.

Keywords:

anterior insular cortex; reward expectancy; temporal structure; phase-precession-like effect; phase-amplitude coupling; reward-specific pattern; intracranial electroencephalography

Introduction

Many daily behaviors of humans are driven by the expectancy of rewards, whether effortless or laborious (Pessiglione et al., 2007; Rowe et al., 2008). Reward expectancy has been proposed to boost behavioral performance via the so-called proactive control, in which rewards are allocated more attentional resources for their salience from contextual information (Frömer et al., 2021; Molnar-Szakacs & Uddin, 2022; Rowe et al., 2008). Of note, the process of identifying salience incorporates the involvement of the salience network (Seeley et al., 2007). As a critical component of the salience network, the anterior insula cortex (AIC) activates ahead of other cortex during various cognitive tasks, such as the oddball attention task (Sridharan et al., 2008) and the flanker task (Cai et al., 2016). These preceding neural activities in the AIC are speculated to benefit the allocation of cognitive resources and facilitate the switch between neural networks to serve different cognitive tasks, thereby participating in reward processing. Recently, electrophysiological evidence has revealed neuronal activities related to reward expectancy in the AIC, showing that approximately a quarter of responsive neurons are activated prior to an expected reward (Mizuhiki et al., 2012). Nevertheless, the exact neural mechanism of how the AIC participates in reward expectancy is poorly understood. Exploring the reward expectancy related activities in the AIC might shed light on promoting information processing speed and working efficiency.

Intracranial electroencephalography (iEEG) provides abundant information revealing the rapid brain dynamics during cognitive processes in deep brain regions such as the AIC. Phases of low frequency iEEG oscillations represent distinct neural characteristics implicated in a range of cognitive tasks. For example, gamma activities coupled to the peak of theta oscillations contribute to memory encoding, while that coupled to the trough of theta oscillations participate in memory retrieval (Kragel et al., 2020; Lopes-Dos-Santos et al., 2018). Using transcranial alternating current stimulation over the sensorimotor cortex to induce pronounced gamma activities at the peak of theta oscillations can substantially enhance motor skill acquisition (Akkad et al., 2021). Furthermore, when encoding sequential events, the neural pattern underlying each event is associated with different phases of low-frequency oscillations in the frontal and temporal lobes (Axmacher et al., 2010; Lisman, 2005; Reddy et al., 2021; Siegel et al., 2009; Yang et al., 2021). Such a phase-locking phenomenon is assumed to be the neural foundation of the limited capacity of short-term memory (Axmacher et al., 2010; Freunberger et al., 2011; Lisman, 2005). Understanding the mechanisms underlying these phase-dependent

effects has garnered considerable attention and holds significant research significance in cognitive neuroscience.

The phase-amplitude coupling (PAC) refers to how the phases of low-frequency oscillations modulate the amplitudes of high-frequency activities and is thought to support information integration in the brain (Mariscal et al., 2021). In the present study, we utilized PAC analysis to investigate the neural dynamic during reward expectancy and explore the functional role of theta phases in this process. In rodents and humans, hippocampal place cells and entorhinal grid cells establish a theta phase precession effect, characterized as cells firing at progressively earlier phases of the local theta oscillations when a subject is going through the place field of a corresponding cell (Hafting et al., 2008; Skaggs et al., 1996). Moreover, the phase precession effect relative to a specific goal has also been unveiled for non-spatially tuned neurons in the frontal cortex (Qasim et al., 2021). Researchers have suggested that the phase precession effect reflects the prediction and anticipation of the forthcoming location or event (Qasim et al., 2021; van der Meer & Redish, 2011). So far, the role of phase precession effect in reward expectancy remains unclear.

In this study, we tested presurgical epilepsy patients implanted with depth electrodes for clinical purposes. They were asked to navigate a virtual T-maze during which subjects encountered rewards at pre-defined locations. The period proximity to the appearance of rewards was defined as the reward-expectancy stage. By analyzing iEEG activities in the AIC and hippocampus, we found a strong PAC between theta oscillations and gamma activities before reaching the reward site in the AIC. Interestingly, we found that the gamma power was coupled to progressively earlier theta phases as the number of trials increased, which is similar to the phase precession effect at the microscopic level of brain signals in which single neurons fire at progressively earlier phases of low-frequency oscillations. It was thus termed phase-precession-like effect (PPLE). Meanwhile, neural representations of rewards were pre-activated at the reward-expectancy stage. Again, such pre-activation also showed similar PPLE indicating that the pre-activated time was locked to earlier theta phases in the AIC across trials. Of note, the peak gamma power in the PAC was more often following the pre-reactivation of reward-specific representations in individual trials. We did not find PPLEs when subjects were preparing motor responses or approaching a location in the AIC, or when they were approaching the reward sites in the hippocampus.

Results

The AIC is involved in directing attention and initiating preparation for forthcoming stimuli (Dajani & Uddin, 2015). It plays a unique role in identifying salience and assigning cognitive resources, and is engaged in reward-related processes (Corbetta et al., 2008; Rothkirch et al., 2014). To investigate the electrophysiological mechanisms of the AIC in processing rewards, we tested 12 epilepsy patients with implanted electrodes, and out of these, 8 patients had a total of 24 contacts located at the AIC (18 in the right hemisphere; Figure 1A; Table S1). Subjects were asked to navigate a virtual T-maze and collect rewards while we recorded iEEG activities (Figure 1B-D). To investigate the involvement of the AIC in reward expectancy, we examined iEEG activities time-locked to entering the reward zone (ERZ event) when the reward appeared on the monitor (Figure 1D). We also analyzed iEEG data time-locked to picking up the reward (PR event) and entering the decision zone (EDZ event) as control analyses. There was no difference in the number of trials between different conditions (31.92±2.43 [mean±SD] for ERZ, 32.08±2.47 for PR, and 32.17±2.48 for EDZ; $F_{(2, 33)} = 0.046$, p=0.95; one-way ANOVA; Figure 1E; see *Methods - SEEG Data Acquisition and Preprocessing*). For each trial, subjects' response time (RT) to the rewards were calculated for further analyses (Figure 1F; see *Results - Functional relevance of PPLEs*).

Prevalence of Theta Oscillations in the AIC

Before performing further analyses on the oscillatory data, we first evaluated the presence of meaningful slow oscillations in the AIC. To do this, we identified low-frequency oscillations (LFOs) using the Multiple Oscillation Detection Algorithm (MODAL; see *Methods - Oscillation Detection*) (Watrous et al., 2018) and observed relatively constant and pronounced LFOs for time windows centered around the ERZ event (Figure 2). The most prevalent LFOs fell in theta band (3.5Hz to 7.5Hz), which were detected in 41.70±1.07% (mean ± SD; Figure 2A-E; Figure S1) time bins on average across subjects. We also found other LFOs in alpha (10Hz to 11Hz; 6.95±1.00%) and beta (13.5 Hz to 14 Hz; 4.67±0.51%) bands, which were less prevalent than LFOs from the theta band (Friedman test: $p=3.35\times10^{-4}$; Wilcoxon matched-pairs signed rank test: $ps\leqslant0.009$). As for the trial-level prevalence, LFOs in theta band were detected in almost all trials (99.58±1.18%, [mean ± SD]), which was significantly higher than that of the other LFOs (alpha band: 45.41±6.27%; beta band: 51.34± 6.21%, Friedman test: $p=1.53\times10^{-3}$; Wilcoxon matched-pairs signed rank test: $ps<0.008$; Figure 2F, G). Similar results were found in time windows locked to PR and EDZ events in the AIC, as well as all events in the hippocampus (Figure S1). The prevalence of theta oscillations is consistent with previous findings showing theta activities in various brain regions

during virtual navigation (Bohbot et al., 2017; Kahana et al., 1999; Watrous et al., 2018) and spontaneous theta oscillations in the insula under the resting state (Das et al., 2022).

Coupling between Theta Phases and Gamma Amplitudes in the AIC when Approaching Rewards

To estimate the neural dynamic of the AIC during reward expectancy, we performed PAC analysis. The time course of phases for each low frequency ($frequency_{low}$;1-15Hz with 1 Hz as a step) and the time course of amplitudes for each high frequency ($frequency_{high}$; 30-150Hz with 5 Hz as a step) were extracted separately for time windows before and after entering the reward zone (pre- and post-ERZ events) for each trial. The PAC strength was calculated between each low-frequency and each high-frequency separately for pre- and post-ERZ events within each trial. Using the multilevel linear regression analysis by considering the variance at contact and subject levels, we computed the difference of the PAC values between pre- and post-ERZ events for each $frequency_{low}$-$frequency_{high}$ pair. To correct errors caused by multiple comparisons, we used a cluster-based permutation analysis to extract $frequency_{low}$-$frequency_{high}$ clusters showing significant coupling when subjects were approaching the rewards (Zhang, 2023) (see *Methods - Phase Amplitude Coupling Analysis*). We found that the coupling between theta phases (5-7 Hz) and gamma amplitudes (80-105 Hz) was stronger during pre-ERZ events compared to post-ERZ events ($p_{corrected}$ = 0.047, Figure 3A). We applied the same analysis to control conditions (i.e., pre-PR and pre-EDZ events) in AIC contacts and to all conditions in the hippocampal contacts but did not find any meaningful clusters. Specifically, two significant PAC clusters were observed in the pre-PR period in the hippocampus (Figure S2A). However, the low frequencies of these clusters were outside the oscillations detected using MODEL and therefore these clusters were considered meaningless.

It's plausible that the coupling between theta phases and gamma amplitudes observed within the AIC during pre-ERZ periods was valued. To further verify the finding, we adopted an ROI approach to scrutinize the PAC strength locked to different events in the AIC and hippocampus. To do this, we extracted the PAC values from the cluster showing an enhanced PAC in the AIC when approaching the reward (Figure 3A) separately for time windows before and after each event for each contact. We then performed a paired t-test of the averaged PAC strength between before and after ERZ events across subjects and found a stronger PAC effect during pre-ERZ periods than post-ERZ periods in the AIC ($t(7) = 3.71$, $p=0.0075$, Figure 3B) but no difference in the hippocampus ($t(6) = 0.04$, $p=0.97$). As for the conditions of PR and EDZ, no difference was observed in either the AIC or the hippocampus ($ts < 2.38$, $ps>0.055$; Figure S2B). Taken together, these results suggest a strong PAC effect between gamma amplitudes and theta phases when subjects are approaching rewards, specifically for contacts located in the AIC.

Additionally, we performed a control analysis by concatenating pre-ERZ periods from all trials together and computed the PAC strength from the concatenated data. Interestingly, no significant PAC cluster was found (ps>0.89). It suggests that the PAC effect varies over trials, causing the PAC effect to disappear in the concatenated data. The variability of PAC effects over trials could arise from two sources. First, distinct gamma frequency bands may exhibit coupling with theta phases across different trials. Second, the coupling of gamma power with various theta phases across trials could also contribute to the variance in PAC effects. We tested the first possibility by examining the distribution of the high frequencies with highest gamma power over trials for each contact. None of 24 AIC contacts showed that the peak gamma frequencies were evenly distributed (Chi-square test, $ps < 3.32 \times 10^{-4}$), suggesting that the disappearance of PAC effect in data of concatenating trials was not because of the difference of peak gamma activities over trials, which ruled out the first possibility. In other words, it implies the second possibility that the coupled theta phases vary across trials, which will be further examined in the subsequent section.

Gamma Activities Exhibit Phase-precession-like Effects in the AIC when approaching rewards

The result reported above suggests that gamma activities are coupled to different phases of theta oscillations across trials when subjects are approaching rewards. Hereby we looked further into the PAC data to compute the dynamics of the locked theta phases across trials. Previous studies have reported the phase precession effect that place cells and grid cells activate at progressively earlier phases across theta cycles when subjects are navigating through corresponding place fields (Hafting et al., 2008; Skaggs et al., 1996). Inspiringly, theta phase precession effect related to the reward site has been reported in the ventral striatum of rodents (van der Meer & Redish, 2011). Evidence suggests that high gamma activities are representing single unit activities at the macroscopic level (Belitski et al., 2008; Ray & Maunsell, 2011). We therefore aimed to investigate if gamma activities were coupled to theta phases that systematically shifted forward when subjects were approaching a reward. To this end, we performed a circular-linear regression analysis between the theta phases that gamma activity peaked at during the pre-ERZ periods and the number of trials for individual AIC contacts (Figure 3C; See *Methods - Phase-Precession-Like Effect of Gamma Activities*) (Qasim et al., 2021). The results showed that, when approaching rewards, gamma activities were progressively coupled to an earlier phase of theta oscillations as the number of trials increased in 14 out of 24 AIC contacts (58.33%) from 7 out of 8 subjects (87.5%), manifesting a significant negative correlation between the theta phase of peak gamma activity in each trial and the trial number (all $ps < 10^{-8}$; Binomial test; Figure 3D, E). Such an effect is reminiscent of the phase precession effect (Qasim et al., 2021; van der Meer & Redish, 2011), and is

therefore called the phase-precession-like effect (PPLE). To distinguish it from the other PPLE mentioned below, this PPLE was termed as $PPLE_{PAC}$.

We assumed that the $PPLE_{PAC}$ was related to reward expectancy. Meanwhile, it might also relate to the expectancy of visual stimuli, specific locations, or outcomes of picking up rewards. To determine whether $PPLE_{PAC}$ in the AIC was specifically related to reward expectancy, we compared the prevalence of $PPLE_{PAC}$ of pre-ERZ events with two control conditions (i.e., pre-PR or pre-EDZ events; Figure 3E. The results showed that the presence of $PPLE_{PAC}$ was observed in fewer AIC contacts for pre-PR (16.67% = 4/24, $p = 5\times10^{-6}$, Binomial test) and pre-EDZ (25% = 6/24, $p = 0.0005$) events compared to pre-ERZ events. We observed a similar pattern at subject levels, showing that fewer subjects exhibited $PPLE_{PAC}$ for pre-PR and pre-EDZ events compared with pre-ERZ events (pre-PR: 25% = 2/8, $p = 0.0004$; pre-EDZ: 50% = 4/8, $p = 0.07$). These findings suggested that the $PPLE_{PAC}$ in the AIC is preferred to reward expectancy rather than reward outcomes (i.e., pre-PR events) or non-reward visual stimuli or specific locations (i.e., pre-EDZ events).

To determine if $PPLE_{PAC}$ prior to reward appearance is specific to the AIC, we examined the prevalence of $PPLE_{PAC}$ in contacts located in the hippocampus during the pre-ERZ event (Figure 3D, E). The results showed that fewer contacts exhibited $PPLE_{PAC}$ in the hippocampus compared to that in the AIC (31.58%=6/19; $p = 0.0061$, Binomial test). Additionally, subjects with hippocampal contacts exhibited numerically fewer $PPLE_{PAC}$, compared with those with AIC contacts (57.14% = 4/7; $p = 0.079$). Futhermore, we computed the presence of $PPLE_{PAC}$ in AIC subregions (Figure S3A; see *Methods - Electrode Reconstruction*) and found that the prevalence of $PPLE_{PAC}$ was highest in the dorsal AIC, especially the anterior short gyrus (ASG; Figure S3B-D; see *Supplementary information*). All together, the $PPLE_{PAC}$ reveals that gamma activities peak at progressively earlier theta phases when subjects approaching rewards and such a reward-expectancy-related $PPLE_{PAC}$ is especially prominent in the AIC.

Pre-activation of the Reward-specific brain Patterns Exhibits PPLE in the AIC when approaching rewards

If there was an expectancy of receiving rewards, it was assumed that the brain patterns representing rewards would be pre-activated prior to the onset of actual rewards. We thus investigated the pre-activation of reward-specific representations before reward onset using the representational similarity analysis (RSA) (Zhang et al., 2018). To do this, we first identified reward-specific neural patterns from the post-ERZ period by comparing the neural similarities between the same (i.e., post-ERZ vs. post-ERZ period at different locations) and different (i.e., post-ERZ vs. post-EDZ period) events (Figure 4A; see *Methods - Computing Reward-Specific Brain Patterns*). We observed that neural activities within two distinct time clusters following the onset of a reward were more similar between two post-ERZ events

than between post-ERZ and post-EDZ events. It indicates the presence of reward-specific effects, characterized by the first reward-specific pattern spanning from 1.04 to 1.08 seconds and the second reward-specific pattern occurring from 1.14 to 1.22 seconds locked to the onset of rewards (*ps*<0.001; Figure 4B).

To compute the pre-activation of reward-specific brain patterns, we conducted correlations by examining the neural similarities between pre-ERZ periods and reward-specific brain patterns during post-ERZ periods. To diminish the temporal proximity effect, the correlations between pre- and post-ERZ periods from the same trial were excluded. The Fisher-z transformed correlation values were averaged across pre-ERZ time windows and trials. We found that the similarity between neural patterns of pre-ERZ period and the reward-specific brain patterns was significantly greater than zeros (the first reward-specific pattern: $t_{(756)} = 27.14$, $p<0.001$; the second reward-specific pattern: $t_{(756)} = 27.05$, $p<0.001$; Figure 4C) . This suggests that the reward-specific brain pattern was pre-activated before the onset of rewards. For each trial, the pre-ERZ time window with the largest correlation coefficient was extracted. We subsequently conducted a comparison of the time difference between the maximum pre-activation time and the peak gamma power coupled to the preferred theta phase reported in the above section. Our findings indicated that the peak gamma activities were more likely to occur slightly after the highest pre-activation, specifically within the time range of 0-0.125s (Figure 4D). Furthermore, the probability of this occurrence was significantly higher compared to what was observed in the simulated data (the first reward-specific pattern: 8.72% vs. 6.17%, $p = 0.0034$; the second reward-specific pattern: 12.29% vs. 6.17%, $p = 3.39\times10^{-4}$; Binomial test). The findings provide compelling evidence that the pre-activation of reward-specific representations occurs before the integration of contextual information and the anticipation of forthcoming rewards (Mariscal et al., 2021).

In the end, we examined PPLEs of the pre-activation of reward-specific neural patterns (Qasim et al., 2021). Theta phases of individual trials were extracted from the highest pre-activation time windows mentioned above (Figure 4E; see *Methods - PPLE of the Pre-activation of Reward-Specific Patterns*). For each contact and each reward-specific pattern, we separately performed the circular-linear correlation between trial numbers and the theta phases locked to the highest pre-activation of reward-specific patterns (Figure 4F). PPLEs were observed in 20.83% (5/24) AIC contacts from 50% (4/8) subjects for the pre-activation of the first reward-specific pattern, while in 25% (6/24) AIC contacts from 50% (4/8) subjects for the pre-activation of the second reward-specific pattern, which were all above the chance level (*ps* < 0.006, Binomial test; Figure 4G, H). It suggests that the pre-activation of the reward-specific brain patterns was coupled to earlier theta phases over trials, which was termed as $PPLE_{RSA}$ in order to distinguish it from $PPLE_{PAC}$. If there was PPLE for either reward-specific pattern in a contact or subject, we considered that the contact or subject presented $PPLE_{RSA}$. Overall, the theta phases of the pre-activation windows exhibited $PPLE_{RSA}$ over trials in 41.67% (10/24, $p=10^{-7}$, Binomial test with chance level) AIC contacts from 62.5%

(5/8, p=1.5×10^{-5}) subjects (Figure 4G). Coincidentally, 5 out of 8 subjects were found exhibited both $PPLE_{RSA}$ and $PPLE_{PAC}$. Subjects #4 and #12 only showed $PPLE_{PAC}$, while subject #7 did not exhibit either PPLE. Moreover, $PPLE_{PAC}$ and $PPLE_{RSA}$ exhibited a comparable spatial distribution within the AIC (Figure S3B-D; see *Supplementary information*). Taken together, the reward-specific representations were preactivated preceding the emergence of the peak gamma activities. Similar to PAC data, the pre-activation of reward-specific brain patterns in the AIC exhibited PPLEs. These findings provide further evidence for the role of the AIC in reward expectancy.

Functional relevance of PPLEs

High prevalence of PPLEs in the AIC preceding ERZ event suggests a potential role for PPLEs in reward expectancy. Previous studies have shown that reward anticipation facilitates cognitive performance, such as shortening the response latency (Baruni et al., 2015; Hermoso-Mendizabal et al., 2020). We thus investigated if PPLEs facilitated subjects' responses to rewards. In order to examine the improvement of RT across trials, z-transformed RT was extracted for each trial in each subject (Figure 5A and S4). Trials with a z-score > 3 were excluded from further data analysis. We then performed a linear regression analysis to predict the z-transformed RT of picking up rewards using the number of trials. RTs trended down for all eight subjects as number of trials increased (βs < 0; Table S2 and Figure 5A, S4). We tested the significance level of the pattern of RT decline by performing a surrogate analysis in each subject. Within each permutation we randomly shuffled the labels of trial numbers, computed the linear regression again and obtained a surrogate coefficient. The permutation procedure was repeated 1,000 times and it generated 1,000 surrogate coefficients. We then ranked the empirical coefficient within the distribution of the surrogate coefficients for each subject. We observed a significant decrease in RT with increasing number of trials in five subjects (ps < 0.05), among whom all subjects exhibited $PPLE_{PAC}$ and four subjects exhibited $PPLE_{RSA}$. In the other two subjects exhibiting PPLEs, the z-transformed RT and the number of trials were numerically negatively related to each other (subject #16: β= -0.21, p = 0.13; subject #17: β= -0.04, p = 0.40). As for subject #7, who did not show any PPLEs, RT showed a very slight decrease pattern with the increase of trial numbers (β= -0.01, p = 0.46). The results support the conclusion that the shortened response latency is related to PPLEs in the AIC.

To find further evidence of PPLEs impacting the behavioral performance, we computed the relation between the strength of PPLEs and the magnitude of performance improvement. We first identified the unstandardized coefficients from the linear regression analysis in which we forecasted z-transformed RTs with trial numbers as the parameter of behavioral improvement (Table S2). For each subject, we extracted the mean strength of $PPLE_{PAC}$ from circular-linear correlation coefficients over contacts. We then performed the Spearman's correlation between the parameter of behavioral improvement and the mean

$PPLE_{PAC}$ strength over subjects and found a significant positive correlation (r = 0.71, *p*=0.047; Figure 5B). It suggests that a stronger $PPLE_{PAC}$ relates to a greater improvement in subjects' performance. We performed the similar analysis to $PPLE_{RSA}$ and no significant correlation was found between the behavioral improvement and $PPLE_{RSA}$ strength (the first reward-specific pattern: r=0.017, *p*=0.97; the second reward-specific pattern: r=0.21, *p*=0.62). Furthermore, RT variability is assumed to be the index of a good performance (Epstein et al., 2011). To investigate the influence of PPLEs on RT variability, we computed the coefficient of variation (CV) for RT in each subject and compared CVs between subjects with or without PPLEs in the AIC (Figure 5C). The result showed that the subjects exhibiting $PPLE_{PAC}$ presented more stable performance with significantly smaller CVs than the subject without $PPLE_{PAC}$ (26.43±6.54% [mean±SD] vs. 56.93%; $t_{(6)}$ = -12.35, p=0.001; one-sample t-test with Bootstrap self-sampling). No significant difference was found between subjects with or without $PPLE_{RSA}$ (the first reward-specific pattern: 28.25±7.35% vs. 32.23±17.09%, $t_{(6)}$=2.01, *p*=0.69; the second reward-specific pattern: 30.72±4.63% vs. 29.77±18.29%, $t_{(6)}$=4.38, p=0.91; independent sample t-test with Bootstrap self-sampling). Taken together, PPLEs, especially $PPLE_{PCA}$, are strongly associated with better behavioral performance.

Discussion

Reward expectancy largely facilitates various cognitive processes, such as attention, memory, and decision-making (Baruni et al., 2015; Frömer et al., 2021; Rowe et al., 2008). To explore the neural basis of reward expectancy, we investigated iEEG activities in the AIC when approaching rewards in a virtual T-maze. Firstly, we reported that gamma activities were coupled to different theta phases over trials in the AIC when approaching rewards. Meanwhile, the reward-specific representations were pre-activated when approaching rewards in the AIC. Such pre-activation tended to occur preceding the peak gamma activities in individual trials. Interestingly, both the peak gamma activities and the pre-activation of reward-specific brain patterns were locked to earlier theta phases across repetitions of approaching the same reward, showing PPLEs. Furthermore, PPLEs is functionally relevant, showing that the strength of PPLEs is related to the magnitude of the improvement in behavioral performance. The identification of PPLEs within the AIC provides valuable insights to better understand the neural mechanism underlying reward expectancy.

The functional role of the AIC in reward expectancy

The pre-activation of reward-specific patterns that we observed before subjects entering the same reward zone supports the functional role of the AIC during reward expectancy. Emerging neuroimaging evidence

has revealed that the AIC is involved at the beginning of the anticipation stage of reward processing (Apaydın et al., 2018; O'Doherty et al., 2002; Schneider et al., 2018). Additionally, invasive studies of non-human primates have reported a class of responsive neurons in the AIC that fire in anticipation of an immediate reward (Mizuhiki et al., 2012). Similar to other brain regions within the reward-processing network, the AIC is believed to participate in the reward expectancy via abundant dopamine, which facilitates predicting the occurrence and timing of rewards (Allman et al., 2005; Hurd et al., 2001). Nevertheless, the unique role of the AIC deserves more attention. Concretely, the expectancy related activity in the AIC is independent of reward validity, while other reward-relate areas, such as the anterior cingulate cortex and ventral striatum, respond especially to valid reward cues (Mizuhiki et al., 2012). A convincing explanation is that the AIC is involved in reward expectancy through proactive control (Frömer et al., 2021). With extensive connections to various limbic and neocortical regions, the AIC is recruited in information integration and salience processing, thereby contributing to linking contextual information and reward (Kurth et al., 2010; Mesulam & Mufson, 1982; Molnar-Szakacs & Uddin, 2022; Sun et al., 2020). In the current study, we further observed that the peak gamma activities, where PAC was established, tended to occur shortly after the pre-activation of reward-specific brain patterns in the AIC, prior to the presentation of the actual reward. Based on these findings, we postulate that the reward-specific representations were pre-activated and subsequently integrated with contextual information through PAC (Kok et al., 2014; Mariscal et al., 2021). These results strengthen the evidence for the functional involvement of the AIC in anticipating forthcoming rewards by establishing context-reward association (Sun et al., 2020). Our study provides the first electrophysiological mechanisms in humans of how the AIC participates in reward expectancy.

Phase precession effect of macroscopic brain signals

The phase precession effect is first reported in brain signals at microscopic levels. Specifically, single units are activated in gradually earlier phases over successive theta cycles of sustained local field potentials (Jones & Wilson, 2005; O'Keefe & Recce, 1993). It is considered to be crucial for compressing slower behavioral sequences to faster neural activity (Jones & Wilson, 2005; O'Keefe & Recce, 1993; Reifenstein et al., 2021) and predicting the forthcoming stimuli (Qasim et al., 2021; van der Meer & Redish, 2011). High gamma activities refer to rapid neural oscillations and is a useful proxy measure of single neuron activities at the macroscopic level (Belitski et al., 2008; Ray & Maunsell, 2011). Nevertheless, there is limited evidence for the theta phase precession effect of high gamma activities. Recently, Zheng et al. have investigated the cross-regional theta-gamma interactions during facial perception using the contextual modulation task and have reported a macroscopic-level effect analogous to theta phase precession (Zheng et al., 2022). Inspiringly, our results also unveiled a particular temporal

structure of neural activities at macroscopic level during reward expectancy in the AIC. Specifically, both the peak gamma activities and the pre-activation time of the reward-specific patterns were found to be locked to earlier theta phases across trials. Such forward shift of theta phases is reminiscent of the phase precession effect and termed PPLEs (Akkad et al., 2021; Kragel et al., 2020; Lopes-Dos-Santos et al., 2018; Qasim et al., 2021; Reddy et al., 2021; Yang et al., 2021). Our finding of PPLEs holds important implications for exploring the phase precession effect of neural activities at multiple spatial (from single-unit recordings to high gamma activities and brain patterns) and temporal (from milliseconds to minutes) scales. Nevertheless, the exact relationship between the PPLEs and the phase precession remains unclear, due to lacking simultaneous recordings at micro- and macroscopic levels. Future studies combining macro- and micro-electrodes are valuable to determine whether the PPLEs have the same spatiotemporal distribution and functional role as theta-phase precession.

Expectancies promote behavioral performance

We also made a preliminary exploration of the behavioral significance for PPLEs in the AIC. Results from our study indicate that PPLEs bear a potentially positive influence on behavioral performance, highlighting the important role of reward expectancy (Frömer et al., 2021; Pessiglione et al., 2007; Rowe et al., 2008). Generally speaking, the context-reward association could be established over several successive trials and contribute to quicker and more accurate responses to rewards (Rowe et al., 2008). In the present study, we observed that the reward-specific pattern was pre-activated when subjects approached the identical location (contextual information) where the reward was about to appear. This finding suggests that the association between context (i.e., location and surroundings) and reward was established. Additionally, we found that the pre-activations preceding the forthcoming reward was gradually locked to earlier theta phases and exhibited PPLEs, implying the progressively consolidation of the context-reward association over trials. Being in the context triggers the pre-activation of reward-related brain activity patterns. Once the reward occurs, the external reward information is consistent with the internal status of pre-activated reward-specific brain patterns. As a result, subjects are more likely to exhibit improved performance due to the preceding preparation of the motor response, characterized by quicker response and higher accuracy levels (Kok et al., 2014). Our discovery sheds light on the potential implementation of neuromodulation techniques to enhance PPLEs and thus promote cognitive capabilities. In future research, there exists a remarkable opportunity to craft meticulously refined experimental tasks that encompass a diverse array of rewards. These rewards may comprise not only psychological and material incentives but also encompass variations in their intensity and efficacy. By embracing such rich and multifaceted experimental designs, we can pave the way for a more precise identification of the optimal spatiotemporal characteristics underpinning neural activity associated with

reward expectancy. Consequently, this heightened understanding will empower us to precisely modulate reward expectancy effect and ultimately enhance behavioral performance.

Conclusions

In summary, we reported the pre-activation of reward-specific patterns following PAC effect between theta phase and gamma amplitude during the expectancy period of a forthcoming reward, indicating that the AIC plays a crucial role in reward expectancy. Further, we identified the neural pattern of PPLEs showing that both the peak gamma activities and the pre-activation time of reward-specific patterns progressively coupled to an earlier phase of the theta oscillations as the number of trials increased. The PPLEs were considered the unique underlying mechanism of the AIC in regulating reward expectancy. More importantly, this neural mechanism is suggested to boost behavioral performance.

Methods

Subject Details

Twelve medically refractory epilepsy patients with depth electrodes for diagnosis (half males; average age = 25.25±8.87 years [mean±SD]; Table S1) were recruited from the Hôpital de la Salpêtrière in Paris and the Second Affiliated Hospital of Zhejiang University in China. The study was approved by the Medical Ethics Committee at the hospital sites, and written informed consent was obtained from all subjects.

Experimental Design

We built a virtual T-maze (Panda3d and PandaEPL) in which subjects could freely navigate. As illustrated in Figure 1B, the T-maze consisted of 2 lateral roads, a central road, a starting zone, a decision zone, and three reward zones. The starting zone was both the beginning and the end of each trial. At the decision zone, subjects chose the correct direction to the lateral road according to the sign on the wall (circle or triangle represents left-turn or right-turn, respectively, Figure 1C, D). Among three reward zones, one was on the central road where a gold coin (value of 0.25 Euros) definitely appeared, and two were on the lateral roads where a gold coin appeared only if subjects chose the correct direction at the decision zone. Once the gold coin appeared, subjects were encouraged to press the Enter button to pick it up. Otherwise, the reward disappeared after subjects navigated through the reward zone. Subjects were encouraged to collect enough gold coins (15 Euros) as soon as possible. To avoid being disoriented, subjects were asked to memorize as many pictures hanging on the wall as possible to encourage them to pay attention to the task and their on-going position. Furthermore,

different paintings of wallpapers also helped subjects to allocate themselves inside the maze to avoid being disoriented (as indicated in Figure 1D). We tested their knowledge about the location of pictures at the end of the experiment.

During the experiment, subjects were lying in their beds with a laptop on a table in front of them. They used arrow buttons on the keyboard to navigate the virtual maze. The full linear running speed was 6 virtual units/second and the linear acceleration speed was 40 virtual units/second^2. The distance from the center of the starting zone to the center of the decision zone was 32 virtual units (Figure 1B). The distance from the center of the left arm to the center of the right arm was 24 virtual units. The width of the corridor was 4 virtual units. Every time subjects picked up the reward or entered the decision zone, they paused for 2 seconds before continuing navigating. The left- and right-turn signs at the decision zone were counter-balanced within each subject. During the experiment, the testing laptop sent triggers to iEEG data in order to synchronize behavioral and iEEG data offline.

Experimental Procedure

At the beginning of each trial, subjects were standing at the starting location (Figure 1D). They first navigated through the middle arm of the T-maze toward the decision zone. On the middle arm, they encountered the first reward. Subsequently, subjects proceeded to enter the decision zone located at the other end of the middle corridor. Immediately after entering the decision zone, a sign of either a triangle or a circle appeared on the wall. Subjects were asked to turn to the correct lateral arm in order to pick up the second reward of that trial. If they made a wrong choice at the decision zone, the second reward of that trial would not appear. At the end of each trial, they navigated back to the starting zone for the next trial. Before the experiment, subjects performed a practical session by going through a different maze to familiarize themselves with the procedure of the experiment and navigating in the virtual environment.

Behavioral Data Collection and Process

During the experiment, the navigating trajectories of subjects were logged. We focused on three events as three experimental conditions for further behavioral and iEEG data analysis: entering the reward zone (ERZ), picking up the reward (PR) and entering the decision zone (EDZ). When subjects entered the reward zone (ERZ), a gold coin would appear on the monitor. The event corresponding to PR was time-locked to the moment when subjects pressed the Enter button to collect rewards. Additionally, upon EDZ, a picture would be displayed on the wall. To match the trial numbers between three conditions, the ERZ and PR events were extracted from the reward zone on the central corridor. Another reason of focusing on the ERZ events located on the central corridor was that subjects' expectancy to this reward never failed. The events of PR on the

central corridor and EDZ were analyzed as control events. The response latency for picking up a reward refers to the time interval between the appearance of a gold coin and the button press to collect the coin in each trial (Figure 1F and S4).

Electrode Reconstruction

Each depth electrode had a diameter of 0.8 mm, with 8-16 contacts. Each contact was 2mm long and 1.5cm apart from the nearest contact on the same electrode. Contacts located in the AIC and hippocampus, known to have close associations with reward processing and spatial memory (Kragel et al., 2020; Lopes-Dos-Santos et al., 2018; Rothkirch et al., 2014), were selected for further data analyses (Figure 1A). The AIC was defined as the part of the insular that precedes the central insular sulcus. It was divided further into four subregions according to the sulci: the anterior short gyrus (ASG), middle short gyrus (MSG), posterior short gyrus (PSG) and anterior inferior cortex (Faillenot et al., 2017) (Figure S3A). The three short gyri were collectively known as the dorsal AIC, while the anterior inferior cortex was considered the ventral AIC (Fathy et al., 2020). The exact location of each contact in the AIC subregions was defined via visual inspection in the local space of each subject using FSLeyes (https://fsl.fmrib.ox.ac.uk/fsl/fslwiki/FSLeyes).

After removing contacts at seizure onset zones and highly contaminated by epileptic spikes, we obtained 24 AIC contacts (18 in the right hemisphere) from 8 subjects and 19 hippocampal contacts (10 in the right hemisphere) from 7 subjects (Figure 1A and Table S1). Three subjects (subject #8, #14 and #15) had both AIC and hippocampal contacts.

IEEG Data Acquisition and Preprocessing

IEEG data was acquired using a Neurolynx system (the Hôpital de la Salpêtrière) and a Nihon-Kohden recording system (the Second Affiliated Hospital of Zhejiang University) in a bipolar layout at sampling rates ≥1k Hz (Table 1). IEEG data were first down-sampled to 1k Hz, bandpass filtered from 0.01 to 200 Hz, and notch filtered at 50 Hz and its harmonics. The filtered data were then re-referenced to the average activity of all depth electrodes outside seizure onset zones (Zhang et al., 2018). We segmented the iEEG data into epochs, spanning 2 seconds before and 2 seconds after each event of interest (i.e., ERZ, PR and EDZ). To remove any edge effects caused by time-frequency decomposition, an extra one second before and after the end of each epoch was extracted. Data preprocessing was performed using EEGLAB toolbox (Delorme & Makeig, 2004) and customized MATLAB code.

The valid epochs were screened for each experimental condition, respectively. Epochs with breaks for clinical purposes (1 epoch from subject #8 under the ERZ condition), missing rewards (i.e., running out of the reward zone without picking up the reward; 1 epoch from subject #15 under the PR condition), and incorrect responses

at the decision zone (4 epochs from subject #16 and 1 epoch from subject #17 under the EDZ condition) were excluded. Epochs contaminated by artifacts such as epileptic activities were detected by visual inspection and excluded from further data analysis. The numbers of trials included were 31.92±2.43 (mean±SD) for ERZ, 32.08±2.47 for PR, and 32.17±2.48 for EDZ, while the numbers of trials excluded were 4.25±2.83 for ERZ, 3.83±2.69 for PR, and 3.67±2.10 for EDZ.

Oscillation Detection

Using the Multiple Oscillation Detection Algorithm (MODAL) (Watrous et al., 2018), we explored the existence of low-frequency oscillations (LFOs) in each epoch for each contact, respectively (Figure 2). Firstly, power spectral density (1–50 Hz in steps of 0.5 Hz) was calculated using Morlet wavelet transformation (6 cycles) for each trial within each contact. Then, a 1/f regression to the background spectrum was constructed in the log-log space, and narrow-band oscillations exceeding the fitted line were identified (Watrous et al., 2018). To evaluate the prevalence of oscillations at each frequency, the percentage of detected time was calculated for each contact and each trial which were further averaged across contacts and trials for each experimental condition and subject (Figure S1).

Phase Amplitude Coupling Analysis

In order to estimate the strength of phase amplitude coupling (PAC), we calculated the modulation index based on the mean vector length (mvlMI) (Özkurt & Schnitzler, 2011; Seymour et al., 2017). To this end, we first filtered iEEG data using the finite impulse response (FIR) and obtained the dynamics of each low-frequency band (1-15 Hz in steps of 1 Hz; 15 samples; $\text{frequency}_{\text{low}}$) and each gamma band (30–150 Hz in steps of 5 Hz; 25 samples; $\text{frequency}_{\text{high}}$) for each ERZ trial (Delorme & Makeig, 2004). The instantaneous phases of the low frequency (ϕ) and the amplitudes of the high frequency (A) were extracted using the Hilbert transformation. We then computed the mvlMI metrics between the time course of the low-frequency phase and high-frequency power for time windows before and after each ERZ event separately using the formula as follows:

$$\text{mvlMI} = \frac{1}{\sqrt{tw}} \frac{\left|\frac{1}{tw}\sum_{t=1}^{tw} A(t) \times e^{i \times \phi(t)}\right|}{\sqrt{\frac{1}{tw}\sum_{t=1}^{tw} A(t)^2}}$$

in which *t* indicates each time point and *tw* indicates the total number of time points. It resulted in two mvlMI metrics (15 $\text{frequency}_{\text{low}}$ × 25 $\text{frequency}_{\text{high}}$) for each ERZ event, one for the pre-ERZ time window and the other for the post-ERZ window. The mvlMI values of pre- and post-ERZ windows were normalized within each trial using a permutation analysis. Within each permutation, we randomly partitioned each epoch (i.e.,

pre- or post-ERZ window) into 2 slices and rearranged their order. We then calculated the mvlMI values of the rearranged data following the same procedure as the empirical data and obtained two surrogate mvlMI metrics. The permutation was repeated 100 times and generated 100 surrogate mvlMI metrics separately for pre- and post-ERZ windows. The normalized mvlMI was calculated by performing a z-transformation of the empirical mvlMI in the surrogate mvlMI distribution (Andrade-Valenca et al., 2011; Özkurt & Schnitzler, 2011) separately for pre- and post-ERZ windows. We then compared the normalized mvlMI values between pre- and post-ERZ periods using a multi-level linear regression analysis by considering the variance at both the subject and contact levels for each $\text{frequency}_{\text{low}}$-$\text{frequency}_{\text{high}}$ bin. Bins corresponding to a p level smaller than 0.05 were selected (Zhang et al., 2015). Adjacent bins were clustered together. The statistical value of each mvlMI cluster was the summed t value from the multi-level linear regression analysis. The significance level of the empirical mvlMI clusters was estimated using a cluster-based permutation analysis (Zhang, 2023). Within each permutation, we randomly shuffled condition labels (i.e., pre- or post-ERZ event) and performed the same multi-level linear regression analysis. It generated a set of permuted mvlMI clusters. The mvlMI cluster with the largest statistical value was selected. The surrogate procedure was repeated 500 times and generated 500 surrogate mvlMI clusters. The significant level of each empirical mvlMI cluster was estimated by ranking its statistical value within the distribution of 500 surrogate mvlMI clusters. If the statistical value of a cluster exceeded the 95th percentile of the surrogate mvlMI distribution, it was labeled as a significant cluster ($p<0.05$). We applied the same analysis to the PR and EDZ conditions in electrodes located at the AIC and hippocampus (Figure 3, S2).

Phase-Precession-Like Effect (PPLE) of Gamma Activities

To estimate the role of PAC in reward expectancy, we examined the phase-precession-like effect (PPLE) by computing the dynamic of the low-frequency phases at which the high-frequency power peaked over trials. To this end, We first extracted the preferred low-frequency phases of the PAC analysis for the time window before each ERZ event. The ϕ_{PAC} was obtained using the following formula,

$$\phi_{\text{PAC}} = \text{angle}\left(\sum_{t=1}^{tw}\left(A(t)^2 \times \cos\left(\phi(t)\right) + A(t)^2 \times \sin(\phi(t)) \times i\right)\right)$$

in which t indicates each time point, tw indicates the total number of time points, A indicates the instantaneous amplitude of the high-frequency band, and ϕ indicates the instantaneous phase of the low-frequency band. It generated one ϕ_{PAC} for each ERZ event within each contact. We then conducted a circular-linear correlation within each contact (Qasim et al., 2021), in which the number of trials was taken as a linear parameter and the ϕ_{PAC} derived from the corresponding trial was taken as a circular parameter. The significance level of the coefficient value was estimated by performing a surrogate analysis. Within each permutation, we randomly shuffled trial labels and then computed the circular-linear correlation again (Zhang, 2023). It generated one surrogate coefficient value. The permutation was repeated 1,000 times and we obtained 1,000 surrogate

coefficient values. If the circular-linear correlation coefficient derived from the empirical data exceeded the 95th percentile of the surrogate coefficient distribution, the empirical correlation value was considered significant, indicating the existence of PPLEs. We performed a control analysis by applying the same analysis to time windows before the PR and EDZ events in contacts of the AIC and hippocampus.

Computing Reward-Specific Brain Patterns

To illustrate neural activities before the reward appearing is relevant to reward expectancy, we computed if the reward representations was pre-activated before reward onset using representational similarity analysis (RSA) (Figure 4A) (Zhang et al., 2018). We first identified the reward-specific brain patterns by analyzing post-ERZ events at different spatial locations, including the mid-arm, the left arm, and right arm. To do this, each post-ERZ event was segmented into 100ms windows with 20ms overlap. Thus, 96 windows were obtained for each post-ERZ period. For each time window, the iEEG power of low-frequency bands (1-30 Hz in steps of 1 Hz) and high-frequency bands (35–150 Hz in steps of 5 Hz) were concatenated (54 frequencies). It resulted in a 54(frequency bins) × 96 (time bins) matrix for each post-ERZ event for each contact. Then, we computed the neural activity similarity between each post-ERZ-post-ERZ pair. To do this, each time window of one post-ERZ trial (trial 1) and every time window of another post-ERZ trial (trial 2) by performing Spearman's correlations over frequencies. Fisher-z transformed correlation coefficients were averaged across all time windows of trial 2. We repeated the same procedure for all time windows of trial 1 and obtained a 1 × 96 (post-ERZ time bins) confusion matrix for each post-ERZ-post-ERZ pair and each contact (RSA_{same}). Note that we excluded correlation coefficients between same trials and between trials at the same location in order to eliminate the temporal proximity effect and the confounding effect induced by representing the same location. We also extracted the brain pattern of the post-EDZ event and computed the similarity of neural activities between each post-ERZ-post-EDZ pair following the same procedure for each contact (RSA_{diff}). Then, the RSA_{diff} values were averaged across all post-ERZ-post-EDZ pairs within each contact which was considered as baseline. We performed a multi-level linear regression analysis between RSA_{same} and mean RSA_{diff} by considering the variance at both subject and contact levels for each post-ERZ time bin. Empirical clusters were extracted by selecting connected time bins corresponding to $p<0.05$, and the statistical value of each cluster was the summed t value from the multi-level linear regression analysis. Subsequently, a cluster-based permutation analysis was computed by randomly shuffling post-ERZ windows 1,000 times (Zhang, 2023). For each permutation, we performed the same multi-level linear regression analysis and selected the cluster with the largest statistical value as the surrogate cluster. The significance level of the empirical clusters was estimated by ranking their statistical value within the distribution of 1,000 surrogate clusters. It was considered significant only if cluster size derived from the true data exceeded the 95th percentile of the surrogate distribution. And the iEEG activities from time windows showing pronounced post-ERZ-post-ERZ similarities were regarded as the reward-specific patterns.

PPLE of the Pre-activation of Reward-Specific Patterns

If the reward-specific brain patterns were pre-activated, we would expect to observe that the pre-ERZ brain patterns are similar to the reward-specific brain patterns, showing significant positive correlation coefficients. To compute the pre-activation of reward-specific brain patterns during pre-ERZ periods, we performed RSA between brain patterns of each pre-ERZ time bin and the reward-specific brain pattern obtained above (see *Methods – Computing reward-specific brain patterns*) for each contact and trial. It generated a fluctuation of the similarity over pre-ERZ time windows. The Fisher-z transformed correlation coefficients were averaged over pre-ERZ time windows of each trial and contact. We then compared the correlation coefficients against zero using the multilevel linear regression analysis by considering the variance at contact and subject levels. To further investigate the temporal structure of the pre-activation, we performed a similar phase-precession-effect analysis as in the above section. First, we computed the fluctuation of the neural similarity between each pre-ERZ time window and reward-specific brain patterns for each trial and contact. The time window with the largest correlation coefficient was considered the peaked pre-activation time window from which the instantaneous theta phase was extracted. It resulted in one $1 \times n$ (trial) phase matrix for each contact. Using previously established algorithms (Qasim et al., 2021), we conducted a circular-linear correlation between the extracted theta phases and trial numbers across trials within each contact. The significance level of the coefficient value was estimated by performing a surrogate analysis. Within each permutation, we randomly shuffled the pre-ERZ windows and performed the same pipeline as in the empirical data. It generated one surrogate coefficient value. The permutation was repeated 1,000 times and we obtained 1,000 surrogate coefficient values. If the circular-linear correlation coefficient derived from the empirical data exceeded the 95th percentile of the surrogate coefficient distribution, the empirical correlation value was considered significant, indicating the existence of PPLEs.

Acknowledgments

We are grateful to the patients for participating in our study. We thank the EEG technologists and nurses for assisting with data transfer and care of affected individuals during the EEG recording. This work was supported by the National Natural Science Foundation of China (81901319, 81971207 and 82171437) and DFG of Germany (ZH822/1-1).

Reference

Akkad, H., Dupont-Hadwen, J., Kane, E., Evans, C., Barrett, L., Frese, A., Tetkovic, I., Bestmann, S., & Stagg, C. J. (2021). Increasing human motor skill acquisition by driving theta-gamma coupling. *Elife*, *10*. https://doi.org/10.7554/eLife.67355

Allman, J. M., Watson, K. K., Tetreault, N. A., & Hakeem, A. Y. (2005). Intuition and autism: a possible role for Von Economo neurons. *Trends Cogn Sci*, *9*(8), 367-373. https://doi.org/10.1016/j.tics.2005.06.008

Andrade-Valenca, L., Dubeau, F., Mari, F., Zelmann, R., & Gotman, J. (2011). Interictal scalp fast oscillations as a marker of the seizure onset zone. *Neurology*, WNL. 0b013e318228bee318222.

Apaydın, N., Üstün, S., Kale, E. H., Çelikağ, İ., Özgüven, H. D., Baskak, B., & Çiçek, M. (2018). Neural Mechanisms Underlying Time Perception and Reward Anticipation. *Front Hum Neurosci*, *12*, 115. https://doi.org/10.3389/fnhum.2018.00115

Axmacher, N., Henseler, M. M., Jensen, O., Weinreich, I., Elger, C. E., & Fell, J. (2010). Cross-frequency coupling supports multi-item working memory in the human hippocampus. *Proc Natl Acad Sci U S A*, *107*(7), 3228-3233. https://doi.org/10.1073/pnas.0911531107

Baruni, J. K., Lau, B., & Salzman, C. D. (2015). Reward expectation differentially modulates attentional behavior and activity in visual area V4. *Nat Neurosci*, *18*(11), 1656-1663. https://doi.org/10.1038/nn.4141

Belitski, A., Gretton, A., Magri, C., Murayama, Y., Montemurro, M. A., Logothetis, N. K., & Panzeri, S. (2008). Low-frequency local field potentials and spikes in primary visual cortex convey independent visual information. *J Neurosci*, *28*(22), 5696-5709. https://doi.org/10.1523/jneurosci.0009-08.2008

Bohbot, V. D., Copara, M. S., Gotman, J., & Ekstrom, A. D. (2017). Low-frequency theta oscillations in the human hippocampus during real-world and virtual navigation. *Nat Commun*, *8*, 14415. https://doi.org/10.1038/ncomms14415

Cai, W., Chen, T., Ryali, S., Kochalka, J., Li, C. S., & Menon, V. (2016). Causal Interactions Within a Frontal-Cingulate-Parietal Network During Cognitive Control: Convergent Evidence from a Multisite-Multitask Investigation. *Cereb Cortex*, *26*(5), 2140-2153. https://doi.org/10.1093/cercor/bhv046

Corbetta, M., Patel, G., & Shulman, G. L. (2008). The reorienting system of the human brain: from environment to theory of mind. *Neuron*, *58*(3), 306-324. https://doi.org/10.1016/j.neuron.2008.04.017

Dajani, D. R., & Uddin, L. Q. (2015). Demystifying cognitive flexibility: Implications for clinical and developmental neuroscience. *Trends Neurosci*, *38*(9), 571-578. https://doi.org/10.1016/j.tins.2015.07.003

Das, A., Myers, J., Mathura, R., Shofty, B., Metzger, B. A., Bijanki, K., Wu, C., Jacobs, J., & Sheth, S. A. (2022). Spontaneous neuronal oscillations in the human insula are hierarchically organized traveling waves. *Elife*, *11*. https://doi.org/10.7554/eLife.76702

Delorme, A., & Makeig, S. (2004). EEGLAB: an open source toolbox for analysis of single-trial EEG dynamics including independent component analysis. *J Neurosci Methods*, *134*(1), 9-21. https://doi.org/10.1016/j.jneumeth.2003.10.009

Epstein, J. N., Langberg, J. M., Rosen, P. J., Graham, A., Narad, M. E., Antonini, T. N., Brinkman, W. B., Froehlich, T., Simon, J. O., & Altaye, M. (2011). Evidence for higher reaction time variability for children with ADHD on a range of cognitive tasks including reward and event rate manipulations. *Neuropsychology*, *25*(4), 427-441. https://doi.org/10.1037/a0022155

Faillenot, I., Heckemann, R. A., Frot, M., & Hammers, A. (2017). Macroanatomy and 3D probabilistic atlas of the human insula. *Neuroimage*, *150*, 88-98. https://doi.org/10.1016/j.neuroimage.2017.01.073

Fathy, Y. Y., Hepp, D. H., de Jong, F. J., Geurts, J. J. G., Foncke, E. M. J., Berendse, H. W., van de Berg, W. D. J., & Schoonheim, M. M. (2020). Anterior insular network disconnection and cognitive impairment in Parkinson's disease. *Neuroimage Clin*, *28*, 102364. https://doi.org/10.1016/j.nicl.2020.102364

Freunberger, R., Werkle-Bergner, M., Griesmayr, B., Lindenberger, U., & Klimesch, W. (2011). Brain oscillatory correlates of working memory constraints. *Brain Res*, *1375*, 93-102. https://doi.org/10.1016/j.brainres.2010.12.048

Frömer, R., Lin, H., Dean Wolf, C. K., Inzlicht, M., & Shenhav, A. (2021). Expectations of reward and efficacy guide cognitive control allocation. *Nat Commun*, *12*(1), 1030. https://doi.org/10.1038/s41467-021-21315-z

Hafting, T., Fyhn, M., Bonnevie, T., Moser, M. B., & Moser, E. I. (2008). Hippocampus-independent phase precession in entorhinal grid cells. *Nature*, *453*(7199), 1248-1252. https://doi.org/10.1038/nature06957

Hermoso-Mendizabal, A., Hyafil, A., Rueda-Orozco, P. E., Jaramillo, S., Robbe, D., & de la Rocha, J. (2020). Response outcomes gate the impact of expectations on perceptual decisions. *Nat Commun*, *11*(1), 1057. https://doi.org/10.1038/s41467-020-14824-w

Hurd, Y. L., Suzuki, M., & Sedvall, G. C. (2001). D1 and D2 dopamine receptor mRNA expression in whole hemisphere sections of the human brain. *J Chem Neuroanat*, *22*(1-2), 127-137. https://doi.org/10.1016/s0891-0618(01)00122-3

Jones, M. W., & Wilson, M. A. (2005). Phase precession of medial prefrontal cortical activity relative to the hippocampal theta rhythm. *Hippocampus*, *15*(7), 867-873. https://doi.org/10.1002/hipo.20119

Kahana, M. J., Sekuler, R., Caplan, J. B., Kirschen, M., & Madsen, J. R. (1999). Human theta oscillations exhibit task dependence during virtual maze navigation. *Nature*, *399*(6738), 781-784. https://doi.org/10.1038/21645

Kok, P., Failing, M. F., & de Lange, F. P. (2014). Prior expectations evoke stimulus templates in the primary visual cortex. *J Cogn Neurosci*, *26*(7), 1546-1554. https://doi.org/10.1162/jocn_a_00562

Kragel, J. E., VanHaerents, S., Templer, J. W., Schuele, S., Rosenow, J. M., Nilakantan, A. S., & Bridge, D. J. (2020). Hippocampal theta coordinates memory processing during visual exploration. *Elife*, *9*. https://doi.org/10.7554/eLife.52108

Kurth, F., Zilles, K., Fox, P. T., Laird, A. R., & Eickhoff, S. B. (2010). A link between the systems: functional differentiation and integration within the human insula revealed by meta-analysis. *Brain Struct Funct*, *214*(5-6), 519-534. https://doi.org/10.1007/s00429-010-0255-z

Lisman, J. (2005). The theta/gamma discrete phase code occuring during the hippocampal phase precession may be a more general brain coding scheme. *Hippocampus*, *15*(7), 913-922. https://doi.org/10.1002/hipo.20121

Lopes-Dos-Santos, V., van de Ven, G. M., Morley, A., Trouche, S., Campo-Urriza, N., & Dupret, D. (2018). Parsing Hippocampal Theta Oscillations by Nested Spectral Components during Spatial Exploration and Memory-Guided Behavior. *Neuron*, *100*(4), 940-952.e947. https://doi.org/10.1016/j.neuron.2018.09.031

Mariscal, M. G., Levin, A. R., Gabard-Durnam, L. J., Xie, W., Tager-Flusberg, H., & Nelson, C. A. (2021). EEG Phase-Amplitude Coupling Strength and Phase Preference: Association with Age over the First Three Years after Birth. *eNeuro*, *8*(3). https://doi.org/10.1523/eneuro.0264-20.2021

Mesulam, M. M., & Mufson, E. J. (1982). Insula of the old world monkey. III: Efferent cortical output and comments on function. *J Comp Neurol*, *212*(1), 38-52. https://doi.org/10.1002/cne.902120104

Mizuhiki, T., Richmond, B. J., & Shidara, M. (2012). Encoding of reward expectation by monkey anterior insular neurons. *J Neurophysiol*, *107*(11), 2996-3007. https://doi.org/10.1152/jn.00282.2011

Molnar-Szakacs, I., & Uddin, L. Q. (2022). Anterior insula as a gatekeeper of executive control. *Neuroscience and biobehavioral reviews*, *139*, 104736. https://doi.org/10.1016/j.neubiorev.2022.104736

O'Doherty, J. P., Deichmann, R., Critchley, H. D., & Dolan, R. J. (2002). Neural responses during anticipation of a primary taste reward. *Neuron*, *33*(5), 815-826. https://doi.org/10.1016/s0896-6273(02)00603-7

O'Keefe, J., & Recce, M. L. (1993). Phase relationship between hippocampal place units and the EEG theta rhythm. *Hippocampus*, *3*(3), 317-330. https://doi.org/10.1002/hipo.450030307

Özkurt, T. E., & Schnitzler, A. (2011). A critical note on the definition of phase-amplitude cross-frequency coupling. *J Neurosci Methods*, *201*(2), 438-443. https://doi.org/10.1016/j.jneumeth.2011.08.014

Pessiglione, M., Schmidt, L., Draganski, B., Kalisch, R., Lau, H., Dolan, R. J., & Frith, C. D. (2007). How the brain translates money into force: a neuroimaging study of subliminal motivation. *Science*, *316*(5826), 904-906. https://doi.org/10.1126/science.1140459

Qasim, S. E., Fried, I., & Jacobs, J. (2021). Phase precession in the human hippocampus and entorhinal cortex. *Cell*, *184*(12), 3242-3255.e3210. https://doi.org/10.1016/j.cell.2021.04.017

Ray, S., & Maunsell, J. H. (2011). Different origins of gamma rhythm and high-gamma activity in macaque visual cortex. *PLoS Biol*, *9*(4), e1000610. https://doi.org/10.1371/journal.pbio.1000610

Reddy, L., Self, M. W., Zoefel, B., Poncet, M., Possel, J. K., Peters, J. C., Baayen, J. C., Idema, S., VanRullen, R., & Roelfsema, P. R. (2021). Theta-phase dependent neuronal coding during sequence learning in human single neurons. *Nat Commun*, *12*(1), 4839. https://doi.org/10.1038/s41467-021-25150-0

Reifenstein, E. T., Bin Khalid, I., & Kempter, R. (2021). Synaptic learning rules for sequence learning. *Elife*, *10*. https://doi.org/10.7554/eLife.67171

Rothkirch, M., Schmack, K., Deserno, L., Darmohray, D., & Sterzer, P. (2014). Attentional modulation of reward processing in the human brain. *Hum Brain Mapp*, *35*(7), 3036-3051. https://doi.org/10.1002/hbm.22383

Rowe, J. B., Eckstein, D., Braver, T., & Owen, A. M. (2008). How does reward expectation influence cognition in the human brain? *J Cogn Neurosci*, *20*(11), 1980-1992. https://doi.org/10.1162/jocn.2008.20140

Schneider, M., Leuchs, L., Czisch, M., Sämann, P. G., & Spoormaker, V. I. (2018). Disentangling reward anticipation with simultaneous pupillometry / fMRI. *Neuroimage*, *178*, 11-22. https://doi.org/10.1016/j.neuroimage.2018.04.078

Seeley, W. W., Menon, V., Schatzberg, A. F., Keller, J., Glover, G. H., Kenna, H., Reiss, A. L., & Greicius, M. D. (2007). Dissociable intrinsic connectivity networks for salience processing and executive control. *J Neurosci*, *27*(9), 2349-2356. https://doi.org/10.1523/jneurosci.5587-06.2007

Seymour, R. A., Rippon, G., & Kessler, K. (2017). The Detection of Phase Amplitude Coupling during Sensory Processing. *Front Neurosci*, *11*, 487. https://doi.org/10.3389/fnins.2017.00487

Siegel, M., Warden, M. R., & Miller, E. K. (2009). Phase-dependent neuronal coding of objects in short-term memory. *Proc Natl Acad Sci U S A*, *106*(50), 21341-21346. https://doi.org/10.1073/pnas.0908193106

Skaggs, W. E., McNaughton, B. L., Wilson, M. A., & Barnes, C. A. (1996). Theta phase precession in hippocampal neuronal populations and the compression of temporal sequences. *Hippocampus*, *6*(2), 149-172. https://doi.org/10.1002/(sici)1098-1063(1996)6:2<149::Aid-hipo6>3.0.Co;2-k

Sridharan, D., Levitin, D. J., & Menon, V. (2008). A critical role for the right fronto-insular cortex in switching between central-executive and default-mode networks. *Proc Natl Acad Sci U S A*, *105*(34), 12569-12574. https://doi.org/10.1073/pnas.0800005105

Sun, K., Xiao, L., Wu, Y., Zuo, D., Zhang, C., Liu, S., He, Z., Rong, S., Wang, F., & Sun, T. (2020). GABAergic neurons in the insular cortex play an important role in cue-morphine reward memory reconsolidation. *Life Sci*, *254*, 117655. https://doi.org/10.1016/j.lfs.2020.117655

Uddin, L. Q., Kinnison, J., Pessoa, L., & Anderson, M. L. (2014). Beyond the tripartite cognition-emotion-interoception model of the human insular cortex. *J Cogn Neurosci*, *26*(1), 16-27. https://doi.org/10.1162/jocn_a_00462

van der Meer, M. A., & Redish, A. D. (2011). Theta phase precession in rat ventral striatum links place and reward information. *J Neurosci*, *31*(8), 2843-2854. https://doi.org/10.1523/jneurosci.4869-10.2011

Watrous, A. J., Miller, J., Qasim, S. E., Fried, I., & Jacobs, J. (2018). Phase-tuned neuronal firing encodes human contextual representations for navigational goals. *Elife*, *7*. https://doi.org/10.7554/eLife.32554

Yang, A. I., Dikecligil, G. N., Jiang, H., Das, S. R., Stein, J. M., Schuele, S. U., Rosenow, J. M., Davis, K. A., Lucas, T. H., & Gottfried, J. A. (2021). The what and when of olfactory working memory in humans. *Curr Biol*, *31*(20), 4499-4511.e4498. https://doi.org/10.1016/j.cub.2021.08.004

Zhang, H. (2023). How Can I Conduct Surrogate Analyses, and How Should I Shuffle? In N. Axmacher (Ed.), *Intracranial EEG: A Guide for Cognitive Neuroscientists* (pp. 567-577). Springer International Publishing. https://doi.org/10.1007/978-3-031-20910-9_35

Zhang, H., Fell, J., & Axmacher, N. (2018). Electrophysiological mechanisms of human memory consolidation. *Nat Commun*, *9*(1), 4103. https://doi.org/10.1038/s41467-018-06553-y

Zhang, H., Fell, J., Staresina, B. P., Weber, B., Elger, C. E., & Axmacher, N. (2015). Gamma power reductions accompany stimulus-specific representations of dynamic events. *Curr Biol*, *25*(5), 635-640. https://doi.org/10.1016/j.cub.2015.01.011

Zheng, J., Skelin, I., & Lin, J. J. (2022). Neural computations underlying contextual processing in humans. *Cell Rep*, *40*(12), 111395. https://doi.org/10.1016/j.celrep.2022.111395

Graphic abstract

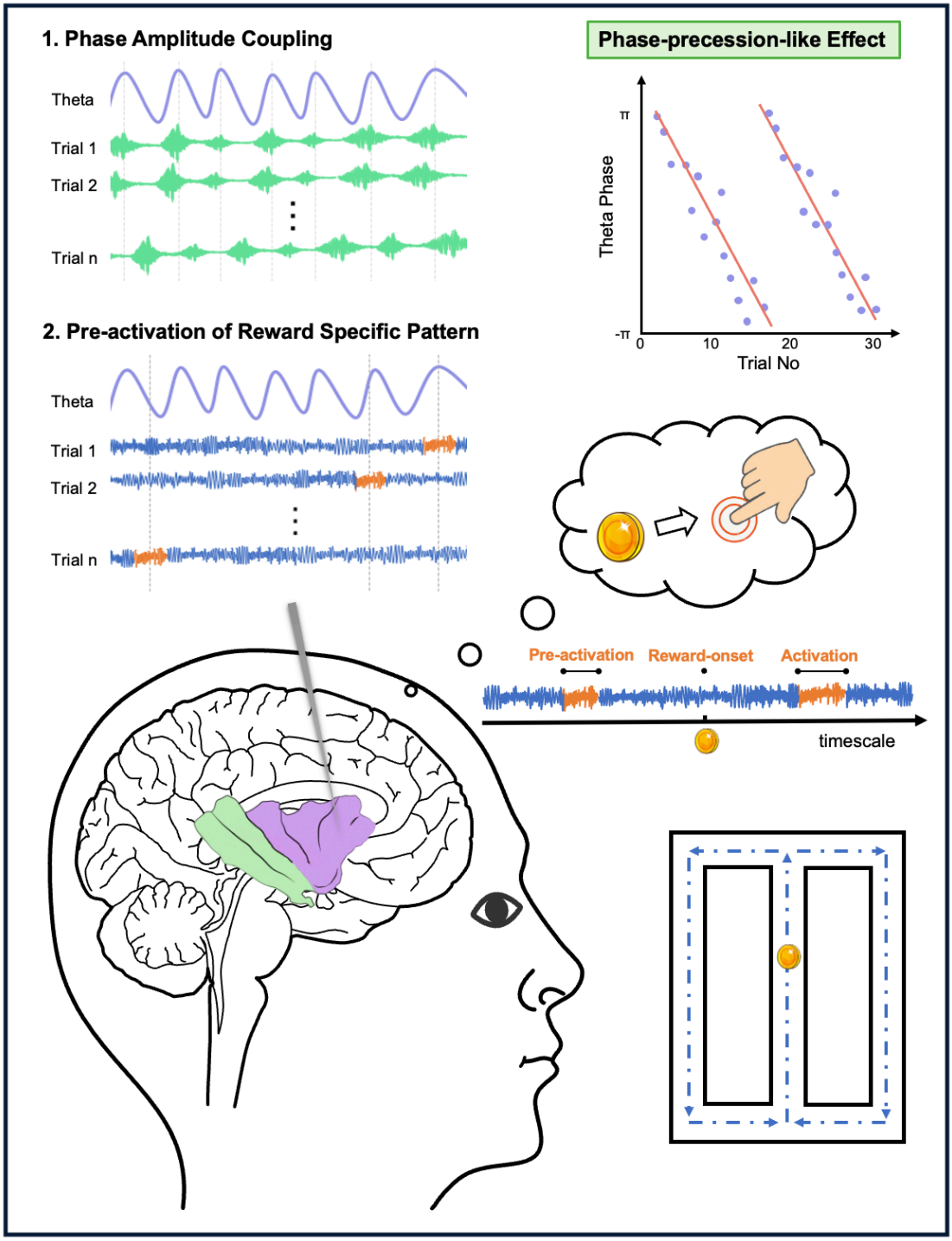

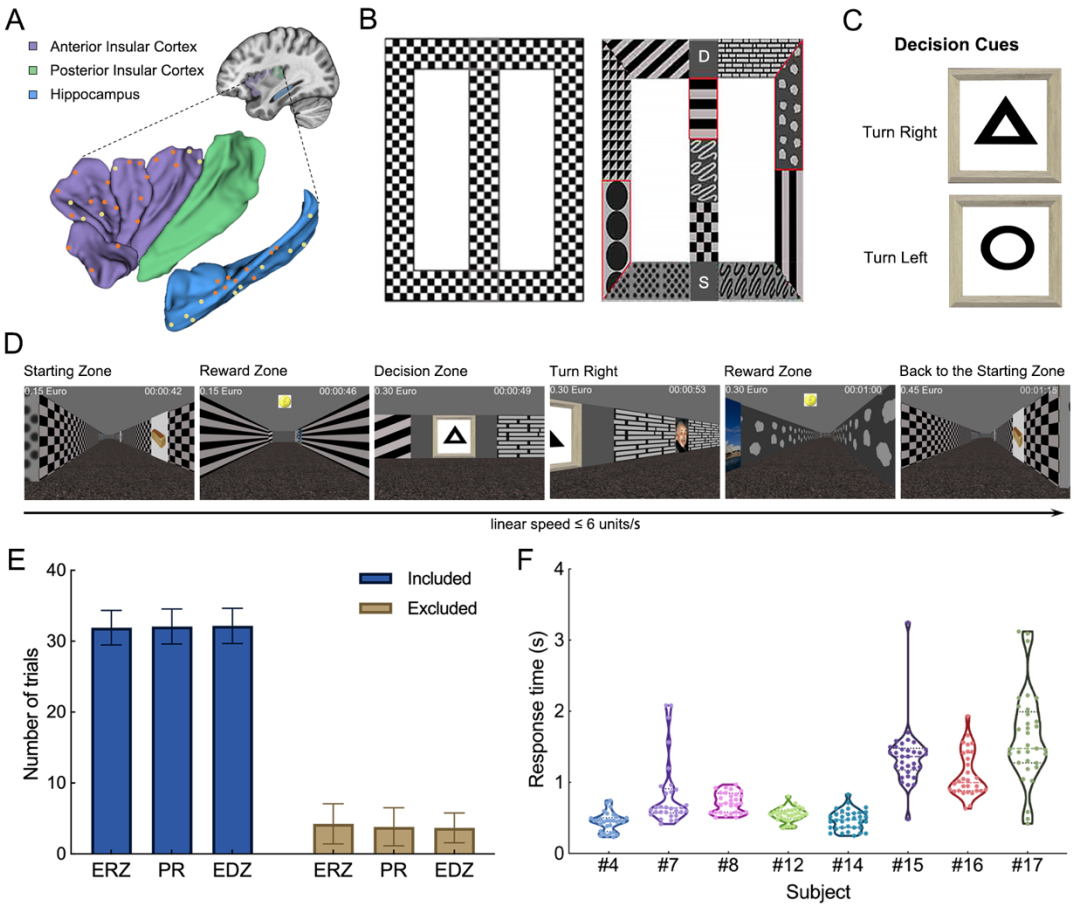

Figure 1. Contact locations, experimental paradigm and behavioral performance.

(A) The 3D view of the anterior insular cortex (AIC, purple), posterior insular cortex (PIC, green), and hippocampus (HPC, blue). For illustration purposes, contacts from both hemispheres are drawn together. Each orange sphere indicates a contact in the right hemisphere, and each yellow sphere indicates that a contact in the left hemisphere. **(B)** Overhead view of the T maze. Left panel: The size diagram of the virtual maze. Each small square represents one square virtual unit. Right panel： The T maze adorned with various patterns on its walls. The gray square marked with "S" represents the starting zone where each trial starts and ends, while the gray square marked with "D" represents the decision zone where subjects are expected to choose the correct direction according to the cue. The areas circled with red lines represent the reward zones, where subjects are expected to press the Enter button to collect gold coins as soon as possible. Otherwise, the reward disappears when they are outside of the reward zone. **(C)** Cues on the wall of the decision zone. Circle represents turning left and triangle represents turning right. **(D)** An example trial viewing from the first-person perspective in the maze. **(E)** Included (dark blue) and excluded (brown) trials separately for each condition. ERZ: entering the reward zone; PZ: picking up the reward; EDZ: entering the decision zone. Error bars indicate one standard deviation (SD) from the mean. **(F)** Behavioral data for subjects with AIC contacts. Each violin plot indicates a subject, and each dot within violin plots indicates a trial.

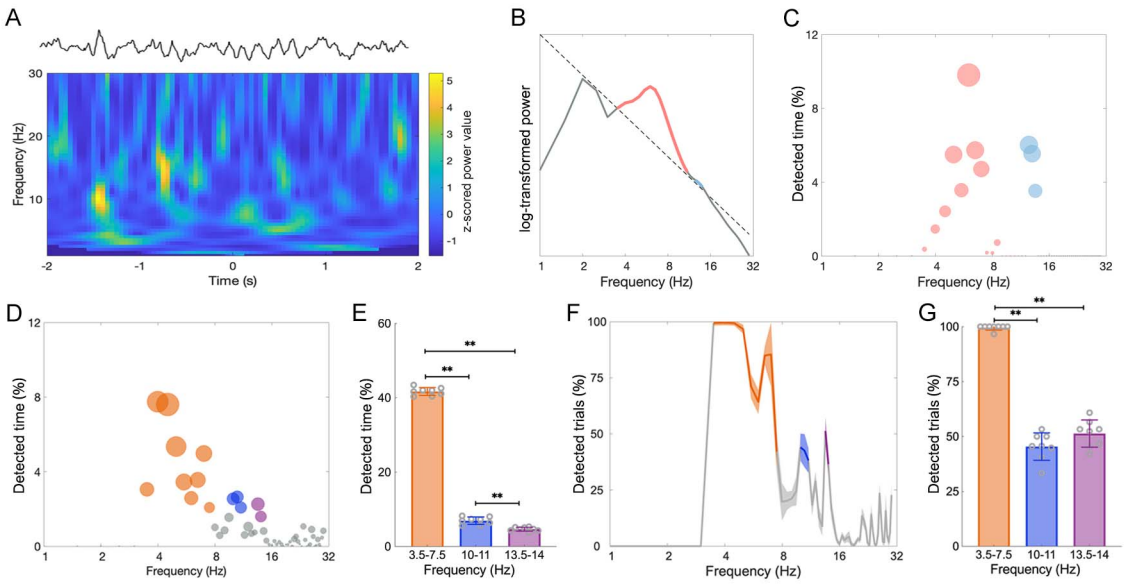

Figure 2. Low frequency oscillations detected in the AIC locked to entering the reward zone.

(A-C) An example trial from a contact located in the right AIC of subject #14. **(A)** The raw trace and its time spectrum diagram of the example trial. Zero represents the timepoint of entering the reward zone. **(B)** Two narrow-band oscillations (3.5-11Hz indicated by the solid pink line; 12.5-14Hz indicated by the solid light blue line) are identified as contiguous frequencies exceeding the fitted line using MODEL(Watrous et al., 2018). **(C)** Prevalence of oscillations at each frequency in panel **(B)**. The larger sphere, the higher percentage of detected time of the corresponding frequency. **(D-G)** Population data for all AIC contacts demonstrating three low frequency oscillations represented by three different colors. Orange indicates 3.5-7.5Hz, dark blue indicates 10-11Hz, purple indicates 13.5-14Hz, and grey indicates frequencies that did not exceed the fitted line using MODAL. **(D)** Percentage of time periods during which oscillatory activities are detected separately for each frequency. **(E)** Proportion of time periods for each detected oscillation band. Gray rings indicate individual subject, the error bar indicates one standard deviation (SD) from the mean, and ** is corresponding to $0.005 \leqslant p < 0.01$. **(F)** The proportion of trials with detected oscillations at each frequency. The shaded area indicates one SD from the mean. **(G)** The proportion of trials in which oscillations are detected in each identified frequency band. Gray rings indicate individual contacts, the error bar indicate one SD from the mean, and ** indicates $0.005 \leqslant p < 0.01$.

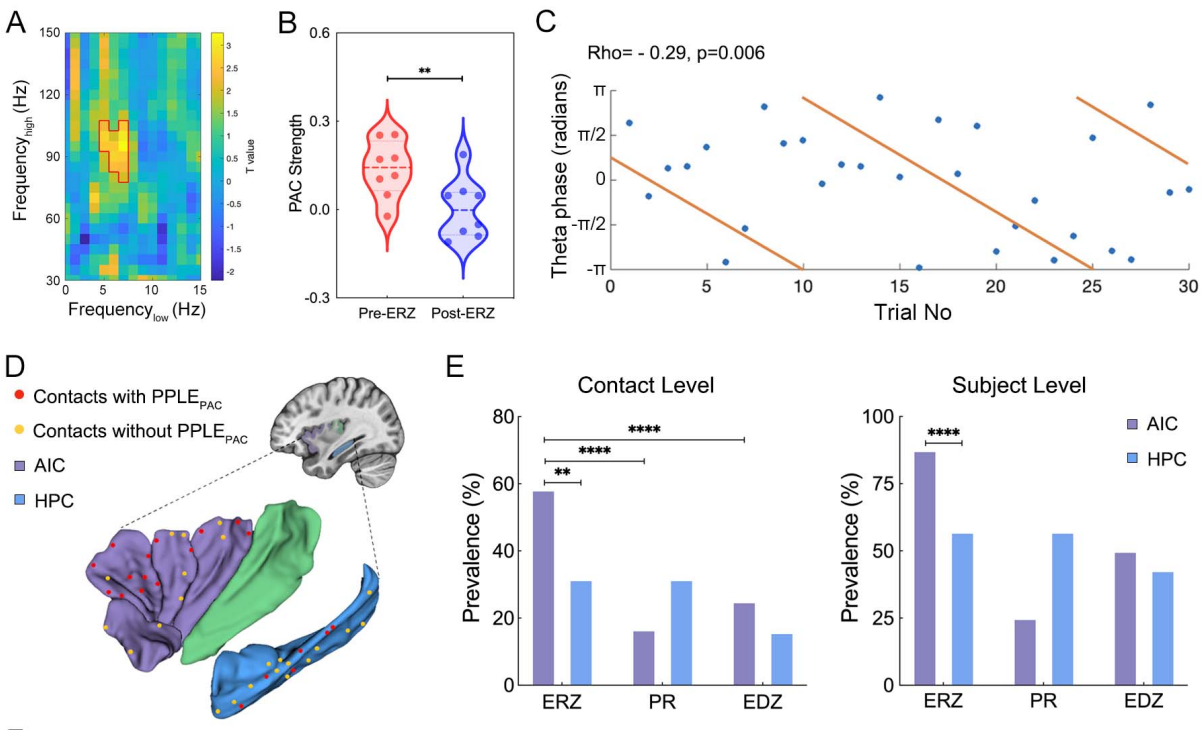

Figure 3. Phase amplitude coupling (PAC) and PPLE$_{PAC}$ before entering reward zones in the AIC.

(A) PAC differences between before and after ERZ event. The frequency$_{low}$-frequency$_{high}$ cluster circled in red lines show enhanced PAC effects for pre-ERZ events than post-ERZ events (Frequency$_{low}$: 5-7Hz; frequency$_{high}$: 80-105Hz). **(B)** Average PAC value within the frequency$_{low}$-frequency$_{high}$ cluster from panel A for individual subjects separately for pre- and post-ERZ events. Each dot indicates one subject, and ** indicates the significance of $0.005 \leq p < 0.01$. ERZ: entering the reward zone. **(C)** An example showing that the peak of gamma power is locked to earlier theta phases over trials when subjects are approaching the reward zone. Blue spheres indicate individual trials and the orange line indicates the fitted line between the preferred theta phase to which gamma activities are coupled and trial numbers. **(D)** Distribution of contacts showing PPLE$_{PAC}$ in the anterior insular cortex (AIC, purple) and hippocampus (HPC, blue). **(E)** Prevalence of PPLE$_{PAC}$ in the AIC and hippocampus for each condition at contact (left panel) and subject (right panel) levels. PR: picking up the reward; EDZ: entering the decision zones. The dashed lines indicate chance level. **: $0.005 \leq p < 0.01$; ****: $p < 0.001$.

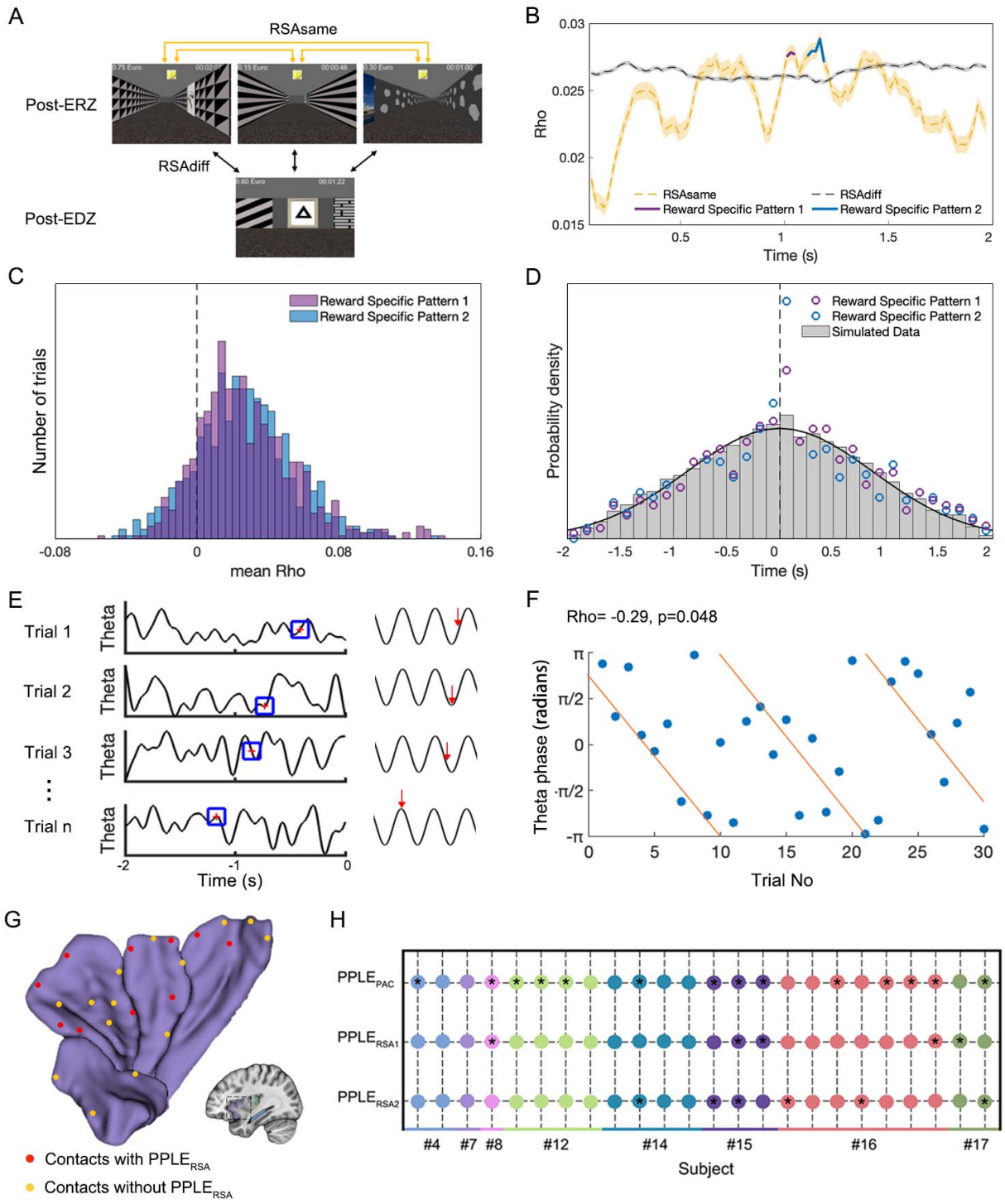

Figure 4. Pre-activation of reward-specific brain patterns and PPLE$_{RSA}$ before entering the reward zones in the AIC.

(A) The concept of computing reward-specific representations. We calculated the similarity of neural patterns between any two post-ERZ-post-ERZ events at different locations (RSA$_{same}$), as well as between post-ERZ and post-EDZ events (RSA$_{diff}$). ERZ: entering the reward zone; EDZ: entering the decision zone. **(B)** Fluctuations of neural similarities of RSA$_{same}$ (indicated by the

yellow dashed line) and RSA_{diff} (indicated by the black dashed line). X axis indicates the time course of post-ERZ period. The solid lines represent the time window of reward-specific patterns, in which the RSA_{same} values are significantly greater than the mean RSA_{diff} values. **(C)** The distribution of correlation coefficients between brain patterns of pre-ERZ time windows and each of the reward-specific representations. **(D)** The probability density of each time interval between the peak gamma activities from the PAC analysis and the peak pre-activation of the first (indicated by blue bars and rings) or second brain patterns (indicated by purple bars and rings). Black line indicates the probability density of the simulated data. Positive numbers represent that the peak gamma activities occur after the pre-activation of reward-specific patterns. **(E)** Theta phases, on which the reward-specific patterns are pre-activated, progressively shift forward across successive trials of a given AIC contact. Each red '+' inside the blue box and the red arrow on the left panel indicate the theta phases of the peak pre-activation time. Time 0 indicates the onset of the reward. **(F)** An example contact exhibiting $PPLE_{RSA}$ before reward appearing. Pre-activation of the reward-specific brain patterns is locked to progressively earlier theta phases over trials, indicating $PPLE_{RSA}$. Each blue sphere indicates one trial. Orange lines indicate the fitted line between trial numbers and theta phases to which the peak pre-activation of reward-specific brain patterns is locked. **(G)** The distribution of contacts exhibiting $PPLE_{RSA}$ in the AIC. **(H)** The overview of AIC contacts showing $PPLE_{PAC}$ and $PPLE_{RSA}$. Each column indicates one contact. Contacts from the same patient are colored the same. '*' indicates significant PPLE after 1,000 permutation tests ($p<0.05$). $PPLE_{RSA\ 1}$ indicates the pre-activation of the first reward-specific brain pattern showing the PPLE effect, and $PPLE_{RSA\ 2}$ indicates the pre-activation of the second reward-specific brain pattern showing the PPLE effect.

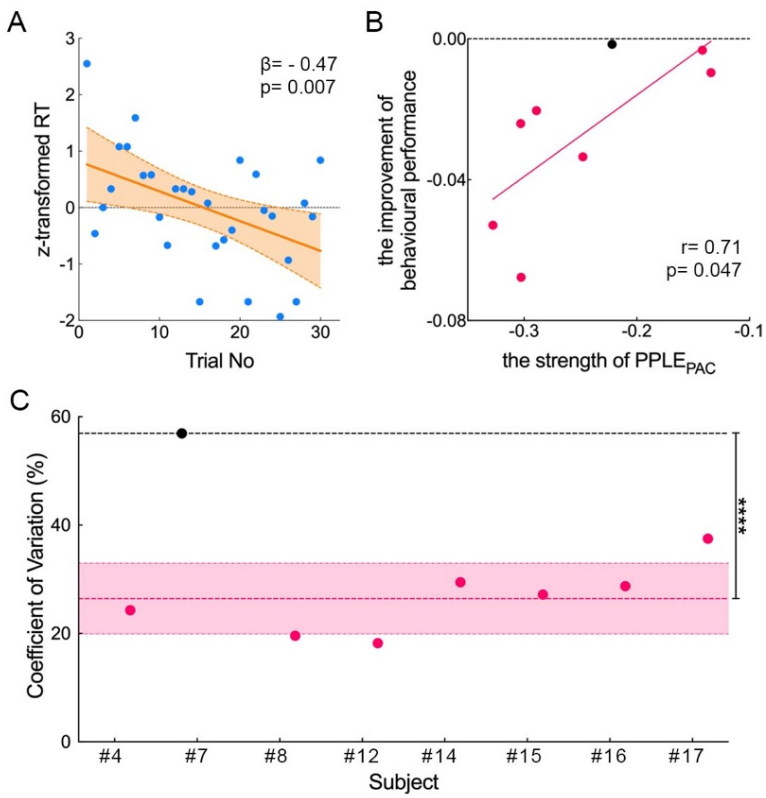

Figure 5. PPLE$_{PAC}$ contribute to the improvement of task performance.

(A) An example showing that the response time (RT) decreases with increased trial numbers. Blue spheres indicate individual trials and the orange line indicates the fitted line between z-transformed RT and trial numbers. Shaded area represents the 95% confidence interval of the fitted line. **(B)** Behavioral performance improved faster for subjects with stronger PPLE$_{PAC}$. Pink spheres indicate individual subjects exhibiting PPLE$_{PAC}$, black sphere indicates the subject without PPLE$_{PAC}$. **(C)** Subjects with AIC contacts showing PPLE$_{PAC}$ (indicated by pink spheres) had significantly less RT variability than the subject without PPLE$_{PAC}$ (indicated by the black sphere). Shaded areas indicate one SD from the mean. ****, $p<0.001$.